https://doi.org/10.5194/egusphere-2023-977
Preprint. Discussion started: 1 June 2023

Investigation of PMSE layers during solar maximum and solar minimum

Dorota Jozwicki[1], Puneet Sharma[2], Devin Huyghebaert[1], and Ingrid Mann[1]

[1]Department of Physics and Technology, UiT the Arctic University of Norway, 9019 Tromso, Norway
[2]Department of Automation and Process Engineering, UiT the Arctic University of Norway, 9019 Tromso, Norway

Correspondence: Jozwicki Dorota (dorota.s.jozwicki@uit.no)

Abstract. Polar Mesospheric Summer Echoes (PMSE) are a phenomenon that are measured in the upper atmosphere during the summer months and can occur in several layers. In this study, we aimed to investigate the relationship between PMSE layers ranging from 80 to 90 km altitude, and the solar cycle. We used 230 hours of observations from the EISCAT VHF radar located near Tromsø, Norway, and applied a previously developed classification model to identify PMSE layers. The observations were taken during the solar maximum of the solar cycle with the years 2013, 2014 and 2015, and during the solar minimum of the solar cycle with the years 2019 and 2020. Our analysis focused on parameters such as the altitude, thickness, and echo power in the PMSE layers, as well as the number of layers present. Our results indicate that the average altitude of PMSE, the echo power in the PMSE and the thickness of the layers is on average higher during solar maximum than during solar minimum. In the considered observations, the electron density at 92 km altitude and the echo power in the PMSE are positively correlated with the thickness of the layers. In addition, we found that higher electron densities at ionospheric altitudes might be necessary to observe multi-layered PMSEs. Furthermore, we observed that the thickness decreases as the number of multi-layers increase. Based on comparisons with previous studies, we hypothesized that the thickness of PMSE layers may be related to the vertical wavelength of gravity waves, with larger wavelengths potentially resulting in thicker layers. Also, an interesting parallel is seen between the thickness of Noctilucent Clouds (NLC) multi layers and PMSE multi layers, where both NLC and PMSE have a similar distribution of layers greater than 1 km in thickness.

1 Introduction

During the summer months, radars can measure a phenomenon in the upper atmosphere called Polar Mesospheric Summer Echoes (PMSE). PMSE are strong radar echoes that are linked to extremely cold temperatures, and they have a characteristic wavy pattern of their height and thickness variation over time. Figure 1 shows a typical example of a PMSE occurrence, where it is possible to notice the variation of altitude an thickness of the PMSE over time. These echoes occur between 80 and 90 kilometers (km) altitude. Their formation requires the presence of turbulence, free electrons, and charged aerosols. The charged aerosols contain water ice, which requires the presence of low temperatures, sufficient water vapor, and nucleation centers to foster heterogeneous condensation, Latteck et al. (2021), Cho and Röttger (1997), Rapp and Lübken (2004). Meteor Smoke Particles (MSP) have been proposed as the likely condensation nuclei, formed through meteor ablation and recondensation.

In addition to MSP, the presence of cold temperatures and water vapor at mid and high latitudes at the mesopause during the summer months creates conditions favorable for ice particle formation Avaste (1993). Cold temperatures and MSPs are known to be at the origin of another phenomenon called Noctilucent Clouds (NLC) Latteck et al. (2021). The combination of neutral air turbulence and negatively charged ice particles results in irregularities in electron density, generating the observed radar echoes or PMSE, at the Bragg wavelength, as described in Latteck et al. (2021).

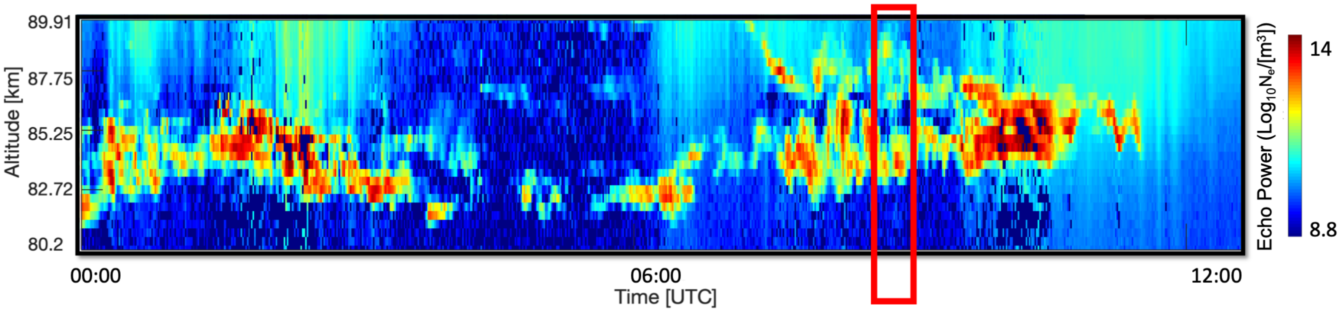

Figure 1. Data from EISCAT VHF from 16 July 2015 from 00:00 to 12:00, showing an example of a PMSE event that contains 3 multi-layers in the red frame.

Multi-layered Polar Mesospheric Summer Echoes (PMSE) have been the focus of several investigations. An example of a PMSE occurrence with three distinct layers is depicted in Figure 1, inside of the red frame. Hoffmann et al. (2005) examined the occurrence and mean altitude of PMSE layers, and performed microphysical model simulations. They proposed that the observed multiple PMSE layer structures are mainly caused by the layering of ice particles due to subsequent nucleation cycles. Li et al. (2016) developed a two-dimensional model to explore the creation process of PMSE. They developed a model able to simulate the presence of gravity waves by assigning both vertical and horizontal wavelengths. They found that increasing the vertical wavelength led to a decrease in the number of layers, while the thickness of the layers increased. Li et al. (2016) also observed that multi-layer formations in their model had preferred altitudes, which were dependent on the size of the ice particles. Additionally, larger particles led to a more rapid decrease in layer altitude and a slower formation.

Some research has also been done on Noctilucent Clouds (NLC), and NLC multilayers. Despite being distinct phenomena, PMSE and NLC have an overlap in the ice particle population that contributes to their formation mechanisms. Lübken et al. (2009) found that NLCs have higher brightness at lower altitudes, while Schäfer et al. (2020) analyzed 182 hours of LIDAR data and found that NLCs occur most of the time in thick layers of more than 1 km. Additionally, they classified the NLCs they observed into 10 subcategories and found that the most frequently occurring subcategory consist of thick layers composed of multiple multi-layers. They report that each of the multi layers move in parallel with each other. This implies that there is a similar movement in the vertical displacement of the multi layers.

Given the significance of electron density in PMSE formation, it is reasonable to expect a potential influence of the solar cycle in it. Limited research has been conducted to examine the connection between multi-layered PMSE and the solar cycle. Zhao et al. (2020) reported a positive correlation between the temperature of the mesopause and the solar flux at 10.7 cm

https://doi.org/10.5194/egusphere-2023-977
Preprint. Discussion started: 1 June 2023

wavelength (F10.7 flux), and found that the height of the mesopause is decreasing with time at polar latitudes. The mesopause, which marks the boundary between the mesosphere and the thermosphere, is characterized by the lowest temperatures in the atmosphere. Such low temperatures at PMSE altitudes are conducive to ice formation, and PMSE are known to be influenced by ice formation through the slowing of diffusion processes. The F10.7 flux is often used as a proxy for the level of solar activity and, more specifically, the amount of ultraviolet radiation that reaches the Earth's upper atmosphere. Shucan et al. (2019) found that PMSE mono, double, and triple layer occurrence ratios are positively correlated with the K index, which corresponds to geomagnetic activity and potential particle precipitation. Also, Shucan et al. (2019) mentions that the PMSE triple layer occurrence ratio shows a negative correlation with F10.7. Narayanan et al. (2022) investigated the effects of particle precipitation on PMSE formation using electron densities from 90 to 95 km, and found that the sudden increase in electron densities due to particle precipitation amplifies the PMSE structures, resulting in an increase in the strength of the backscattered signal.

Understanding the trend of winds and gravity waves at PMSE altitudes is fundamental in comprehending the formation of PMSE. Neutral wind shears generate turbulence which is a key factor in PMSE measurements. Singer et al. (2012) found that westward winds are increasing below an altitude of about 85 km, while eastward winds are increasing above 85 km, particularly during summer. They also found that at an altitude of about 75 km, the long-term trend of zonal winds corresponds to increased activity of gravity waves with periods of 3 to 6 hours at altitudes between 80 km and 88 km. Severe solar proton events cause eastward winds to increase above an altitude of about 85 km. This behavior of winds and gravity waves at PMSE altitudes may be key to better understanding the turbulence at those altitudes leading to the formation of multi-layered PMSE.

Our objective is to analyze the number of PMSE layers, their thickness, altitude, and general behavior during solar maximum and minimum, and to determine possible correlations between these variables and the electron density at ionospheric heights above PMSE. The study is organized as follows: In Sect. 2, we describe the methods and theories related to the pre-selection of the PMSE data, as well as the correlation coefficients employed to assess the significance of our results. In Section 3, we present and discuss the obtained results. Finally, in Sect. 4, we summarize the conclusions drawn from this study.

2 Methods and Theory

In this section, we will provide an overview of the theoretical background behind the formation of PMSE. We will then describe our methodology for data selection, including the tools utilized. Furthermore, we will present the criteria used for identifying the different PMSE layers and the metrics employed for analyzing the collected data.

2.1 Theory behind the formation of PMSE

In this study, we use recorded data from the EISCAT VHF radar located in Tromsø that operates at 224 MHz. EISCAT VHF measures the small scale fluctuations of electrons in the ionospheric plasma. When an electromagnetic wave from EISCAT VHF is transmitted into a portion of the ionosphere, the electric field of the wave causes ionospheric electrons to begin oscillating. The electrons scatter the electromagnetic wave with the same frequency as the incoming wave. This is Thomson scattering.

The distribution of the electron velocities results in the Doppler spectrum observed. This process, called incoherent scatter depends on ionospheric plasma parameters, and one can derive from the observed signal the electron density, and electron and ion temperatures Beynon and Williams (1978). In their study, Rapp and Lübken (2004) elucidate the difference to PMSE, where PMSE are typically stronger than incoherent scatter located at the same altitude, and their spectrum is more narrow.

The PMSE have different spectral characteristics, and they arise due to the combination of several different processes. Gravity waves propagate through the atmosphere and break around the altitude where PMSE form. When these waves break, they create various areas of turbulence, among which some areas would be larger, and some would be smaller. The turbulence structures the present electron content in those areas, as the electrons are coupled to the larger ions in the region that are influenced by the neutral atmospheric motion and turbulence. The radar signal measures the turbulence occurring at scales of half the radar wavelength, Rapp and Lübken (2004). When this happens, the oscillating electrons, governed by the turbulence present in the area, will scatter electromagnetic waves in a similar direction. Constructive interferences will happen, resulting in an amplified backscattered power and a narrower peak in the power spectrum compared to a case without PMSE. Of course, in the case of a portion or ionosphere with PMSE, the resulting power spectrum can have both spectral signatures discussed above: the regular incoherent scatter signal which is broader, as well as the signal that comes from the coherent interferences that would be more narrow.

2.2 Data selection

The Grand Unified Incoherent Scatter Design and Analysis Package (GUISDAP) is a software package used for processing and analyzing data from the EISCAT VHF incoherent scatter radar, Lehtinen and Huuskonen (1996). GUISDAP analysis fits the observed frequency spectrum received from each height with an incoherent scatter profile. The analysis returns the electron density based on the backscattered power, independently from the scattering process. The electron density parameter given by the analysis is proportional to the received echo power and therefore the strength of the PMSE.

We downloaded over 230 hours of recorded data via the Magridal website. This corresponds to 17930 data points, with the details provided in Table 1.The EISCAT VHF radar utilizes multiple experimental modes to collect data. For this study, we specifically analyzed data obtained using the manda code, which is designed to detect low-altitude signals and provides spectral measurements at mesospheric altitudes. We chose a time resolution of 60 seconds and a height resolution of 0.360 km.

We employed EISCAT VHF frequencies over UHF frequencies due to the latter exhibiting a lower recorded amount of PMSE compared to VHF frequencies. As the Heating experiment is known to influence the back-scattered power (also known as echo power) of the PMSE, Belova et al. (2003), we carefully selected data from the days when the Heating experiment was not performed. This enabled us to compare electron densities at 92 km altitude alongside echo power at PMSE altitudes.

The data was carefully selected to encompass the solar maximum and solar minimum phases of the solar cycle. For the purpose of this study, we do not require an absolute value of PMSE strength, thus, we do not perform all the steps that would be necessary to obtain the absolute radar reflectivity as per the study by Hocking et al. (1986).

Table 1. Data-set used for this study. The upper part of the table displays the dates and times selected for the solar maximum, and the lower part of the table is dedicated to the solar minimum. The date and time format are given respectively by the dd/mm/yyyy and the ...h...m format.

	Year	**Date dd/mm/yyyy**	**Start time**	**End time**	**Observation Hours per Day**	**Observation Hours per Year**	**Observation Hours per Solar Max. or Min.**	**Total of Observation Hours**
Solar Maximum	2013	27/06/2013	07h02m	10h58m	03h56m	57h52m	130h18m	230h32m
		28/06/2013	07h02m	12h58m	05h56m			
		09/07/2013	00h00m	00h00m	24h00m			
		10/07/2013	00h00m	00h00m	24h00m			
	2014	23/07/2014	00h00m	09h26m	09h26m	09h26m		
	2015	15/07/2015	08h00m	00h00m	16h00m	63h00m		
		16/07/2015	00h00m	00h00m	24h00m			
		17/07/2015	00h00m	23h00m	23h00m			
Solar Minimum	2019	18/06/2019	06h59m	00h00m	17h00m	59h13m	100h14m	
		19/06/2019	00h00m	12h59m	12h59m			
		04/07/2019	07h07m	12h21m	05h14m			
		20/08/2019	00h00m	00h00m	24h00m			
	2020	06/07/2020	07h58m	09h08m	01h06m	41h01m		
		07/07/2020	00h00m	11h59m	11h59m			
		08/07/2020	00h00m	11h59m	11h59m			
		09/07/2020	00h00m	11h58m	11h58m			
		10/07/2020	08h00m	11h59m	03h59m			

To investigate the behaviour of the ionosphere in relation to PMSE, we compared the echo power for PMSE altitudes between 80 and 90 km, with the electron density at 92 km ionospheric altitude. We used the electron density at 92 km altitude as a reference as it was the closest to the PMSE altitudes and the results were similar for altitudes of 92, 95, and 100 km.

2.3 Data processing

In this paper, we consider two variables: echo power and electron density. Both are measured in base 10 logarithmic units of the number of electrons per cubic meter. The number of electrons per cubic meter is proportional to the back-scattered power for incoherent scatter, where the back-scattered power is defined as the amount of power in the scattered signal received by the antenna. We define the back-scattered power at 92 km altitude as electron density. The back-scattered power at PMSE altitudes, between 80 and 90 km altitude, is defined as echo power.

We selected the PMSE data between 80 and 90 km altitude by using a segmentation model from the study by Jozwicki et al. (2022). The segmentation model used random forests on a set of hand-crafted features to segment the PMSE data from the background. On the output from the segmentation model, we applied a threshold to ensure that only PMSE data were retained

https://doi.org/10.5194/egusphere-2023-977
Preprint. Discussion started: 1 June 2023

for further analysis. This thresholding technique was also employed in the study by Shucan et al. (2019), where they used an echo power threshold $N_e > 2.6 \times 10^{11} m^{-3}$, and in the study by Rauf et al. (2018b), where the authors used a threshold $N_e > 5.0 \times 10^{10} m^{-3}$. We were able to use a lower threshold of $N_e > 3.2 \times 10^{10} m^{-3}$ (which is equivalent to 10.5 in base 10 logarithmic units of the number of electrons per cubic meter) as the segmentation model from the study by Jozwicki et al. (2022) had successfully removed almost all non-PMSE data. This enabled us to retain a large amount of PMSE data per number of hours of observation, in comparison to the findings of Shucan et al. (2019) and Rauf et al. (2018b).

2.4 Detection of PMSE multi-layers

After processing the data at PMSE altitudes as described in Sect. 2.3, we aimed to detect the start and end of each PMSE layer in altitude. To achieve this, we utilized a method used in the study by Hoffmann et al. (2005) and Shucan et al. (2019). This method involves defining the start of a layer each time the threshold for echo power is exceeded, and the end of the layer when the echo power falls below the given threshold. The time intervals and the corresponding altitude intervals associated with the start and end of each layer were recorded. During solar maximum conditions, we observed a maximum of six layers. In this study, we decided to ignore multi layers with more than 4 layers, as their occurrence rates were low. For instance, we observed 13 occurrences of 5 multi layers in the whole data-set, and 2 occurrences of 6 multi layers. In Table 2, we show the occurrences of monolayer and multilayer PMSE events, observed during the solar minimum and solar maximum phases, with each occurrence corresponding to a 1-minute interval.

2.5 Data analysis

In this study, we perform comparisons between the different mono and multi layers of PMSE by using a number of parameters. The parameters included the starting and ending altitude intervals of the layer, the layer thickness (calculated as the difference between the start and end altitude interval), the mean altitude interval that corresponds to the middle of the layer, the echo power in the mean altitude interval inside the PMSE, the altitude of the mean altitude interval, the layer's time interval, the UTC time associated with the time interval, the number of layers present in the time interval, and the electron density at 92 km altitude.

In order to investigate different PMSE properties, we use the Pearson correlation coefficient and the Spearman's rank correlation coefficient to calculate the correlations between the different parameters. The Pearson correlation coefficient is used to measure how strong and in what direction two variables are related in a linear way Wilks (1995). For two random variables X and Y, the Pearson correlation coefficient is defined as follows Wilks (1995):

$$r_{Pearson}(X,Y) = \frac{cov(X,Y)}{\sigma_X \sigma_Y} \tag{1}$$

Where σ_X and σ_Y are the respective standard deviations of X and Y, and cov is the covariance.

The Spearman's rank correlation coefficient is a measure of the strength and direction of the relationship between two variables. It is similar to the Pearson correlation, but instead of measuring the linear relationship between two variables, it

https://doi.org/10.5194/egusphere-2023-977
Preprint. Discussion started: 1 June 2023

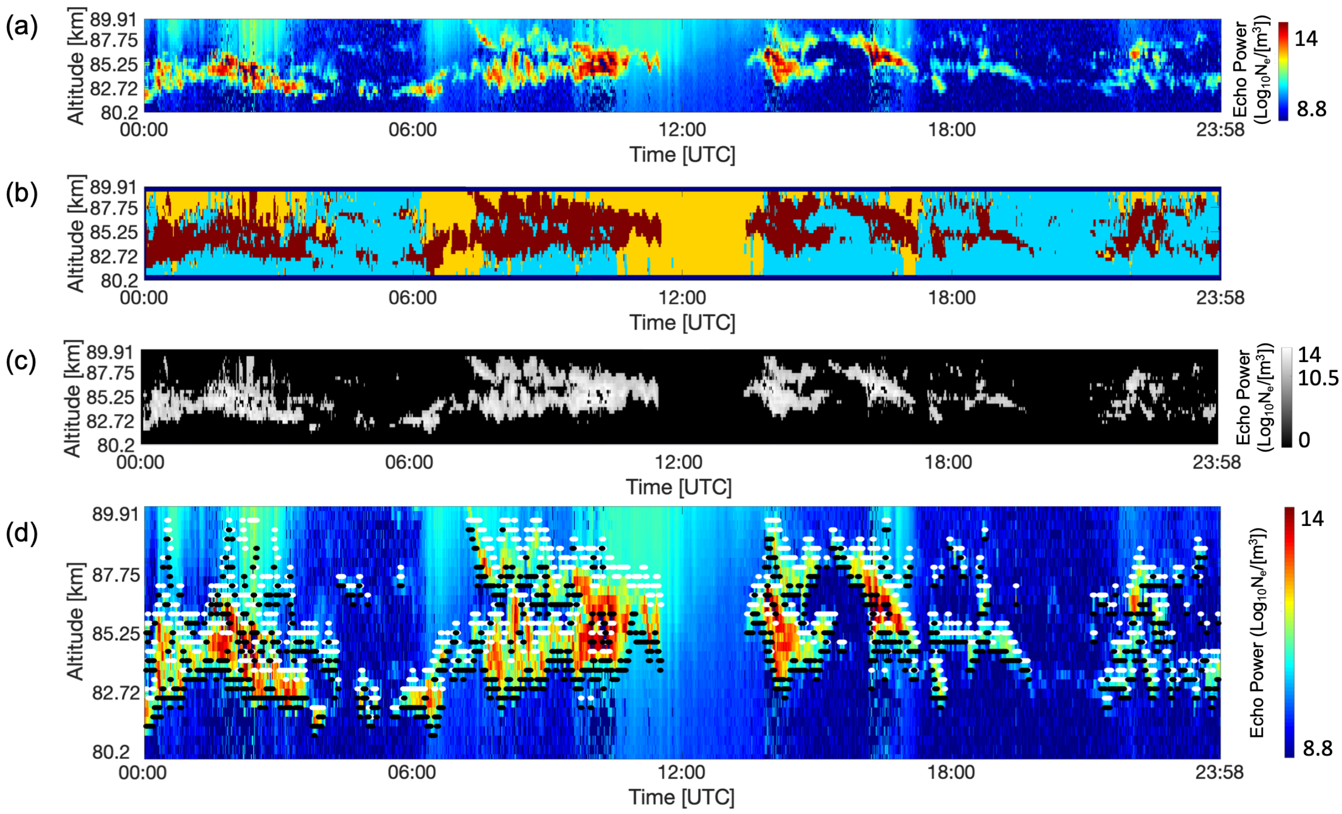

Figure 2. Figure illustrating the process of the layer detection. **(a)** shows the original data for the 16 July 2015 between 00:00 and 23:58. **(b)** shows the output from the classification model used from Jozwicki et al. (2022). Dark red represents areas labeled as PMSE, cyan represents areas of the data labeled as background noise and yellow represents areas labeled as ionospheric background. **(c)** represents the data labeled as PMSE in dark red from sub Fig. 2(b), onto which we applied the threshold described in Sect. 2.3 to make sure we have only PMSE data left. Finally, **(d)** represents the detected beginning and end of layers respectively represented with white and black points, overlayed on the original data.

measures the monotonic relationship between them. The Spearman's rank correlation coefficient is obtained by calculating the Pearson correlation between the ranked values of the variables (Myers and Well, 2003) To compute the Spearman correlation coefficient, for a sample size n, the raw scores Xi and Yi are converted into their rank values rg_X and rg_Y. After that, the Spearman correlation coefficient is then computed as follows:

$$r_{Spearman} = \frac{cov(rg_X, rg_Y)}{\sigma_{rg_X}\sigma_{rg_Y}} \tag{2}$$

Where σ_{rg_X} and σ_{rg_Y} are the standard deviations of the rank variables, and cov(rg_X,rg_Y) is the covariance of those rank variables.

Table 2. This table displays the number of occurrences and approximate percentage of occurrence for each of the mono and multi layers in our data-set. The data is separated by solar maximum and solar minimum. For both solar maximum and solar minimum, the approximate percentage of occurrence for 5 multi layers or more is below one percent. Therefore, the analysis in this study is limited to PMSEs with up to four multi-layers.

		Number of Occurrences	Total Number of Occurences per Sol Max. or Min.	Approximate Pencentage of Occurence
Solar Maximum	Mono Layers	3077	5996	51
	2 Multi Layers	2233		37
	3 Multi Layers	597		10
	4 Multi Layers	81		1
	5 Multi Layers	6		<1
	6 Multi Layers	2		<1
	7 Multi Layers	0		0
Solar Minimum	Mono Layers	1399	2736	51
	2 Multi Layers	935		34
	3 Multi Layers	328		12
	4 Multi Layers	67		2
	5 Multi Layers	7		<1
	6 Multi Layers	0		0
	7 Multi Layers	0		0

3 Results and Discussion

In this section, we will discuss our results which are organized into multiple parts. Firstly, we will discuss the distributions of a few variables, which will be presented using histograms. Subsequently, we will analyze the correlation coefficients that we have computed for the different variables.

3.1 Height distribution of PMSE layers

The average altitude of all layers together is higher during solar maximum than during solar minimum as illustrated in Fig. 3. There is a slight increase in altitude with increasing number of layers in the case of solar maximum seen in Fig.4, but not in the case of solar minimum seen in Fig. 5. Our study confirms the findings of Hoffmann et al. (2005) regarding the altitude of the observed mono layers. They reported that mono layers occurred at an average altitude of 84.8 km, and our results show that the mean altitude of mono layers was 85.21 km for solar maximum and 84.46 km for solar minimum. Our mean altitude of 84.83 km is consistent with the results of Hoffmann et al. (2005). They observed that mono layers occurred 50.1%, double layers 36.6%, and multi layers with more than 2 layers 13.3%, during both solar maximum and minimum periods. Our study indicates that mono layers were observed at a rate of 51% in both solar maximum and minimum, while double layers occurred at a rate of 37% in solar maximum and 34% in solar minimum. Furthermore, we found that the occurrence rate for multi layers with 3 and 4 layers combined was more than 11% in solar maximum and more than 14% in solar minimum. Therefore, our results are consistent with those of Hoffmann et al. (2005) concerning the occurrence rate of mono and multi layers too.

An unexpected result is that during solar maximum, the average altitude of PMSEs is higher than during solar minimum. This is counter-intuitive, as one might expect that during solar maximum, the higher energy of incoming particles from the Sun would result in a lower altitude of PMSEs due to their ability to penetrate further into the atmosphere.

Lübken et al. (2021) show in their study that over time the ice particles are increasing in size. In Fig. 3, we can see that the altitude of the PMSE layers is on average lower for solar minimum compared to solar maximum. This could be due to the fact that the ice particle sizes increase over time, and our selected date for the solar maximum are anterior to the selected dates for the solar minimum. Therefore, it appears that factors other than the sole influence from the solar cycle play a significant role in the altitude of PMSE.

Zhao et al. (2020) found that the height of the mesopause is decreasing with time at polar latitudes over their 18 year long investigation time. Our study focuses on observations from the summer mesopause during solar maximum in years 2013 to 2015, and solar minimum in years 2020 and 2021. We could hypothesize that in the latter years corresponding to solar minimum, the mesopause was lower than during the previous years corresponding to solar maximum. This could have potentially made it possible for PMSE to appear over a wider altitude range during solar minimum, and therefore at lower altitudes. We indeed notice in Fig. 3 that the average altitude of PMSE is slightly lower during solar mimimum, and that the calculated standard deviation is higher during solar minimum compared to solar maximum, which means that the PMSE would indeed be able to form over a wider altitude interval.

3.2 Distribution of the electron density

In the next step we investigate how the distribution of the PMSE layers varies with the ionization observed at the same time. All the observed electrons densities are summarized in Fig. 6; they range from 8.9 to 11.7 electrons per cubic meter in base 10 logarithmic unit during solar maximum and their mean value is slightly higher during solar maximum. Specifically, multi-layer PMSEs with 2 layers exhibit the highest average corresponding electron density, reaching 10.47 electrons per cubic meter in base 10 logarithmic unit as one can see from Fig. 7. In contrast, the mono layers during solar minimum have the lowest average corresponding electron density, with a value of 10.15 electrons per cubic meter in base 10 logarithmic unit, as displayed in Fig. 8. It is worth noting that, for both solar maximum and solar minimum periods, the mono layers corresponded to the lowest average electron density of their respective seasons. However, it is important to bear in mind that this trend is weak and that the standard deviations are quite large. A plausible argument could be made that higher electron densities at ionospheric altitudes might be necessary to observe multi-layered PMSEs.

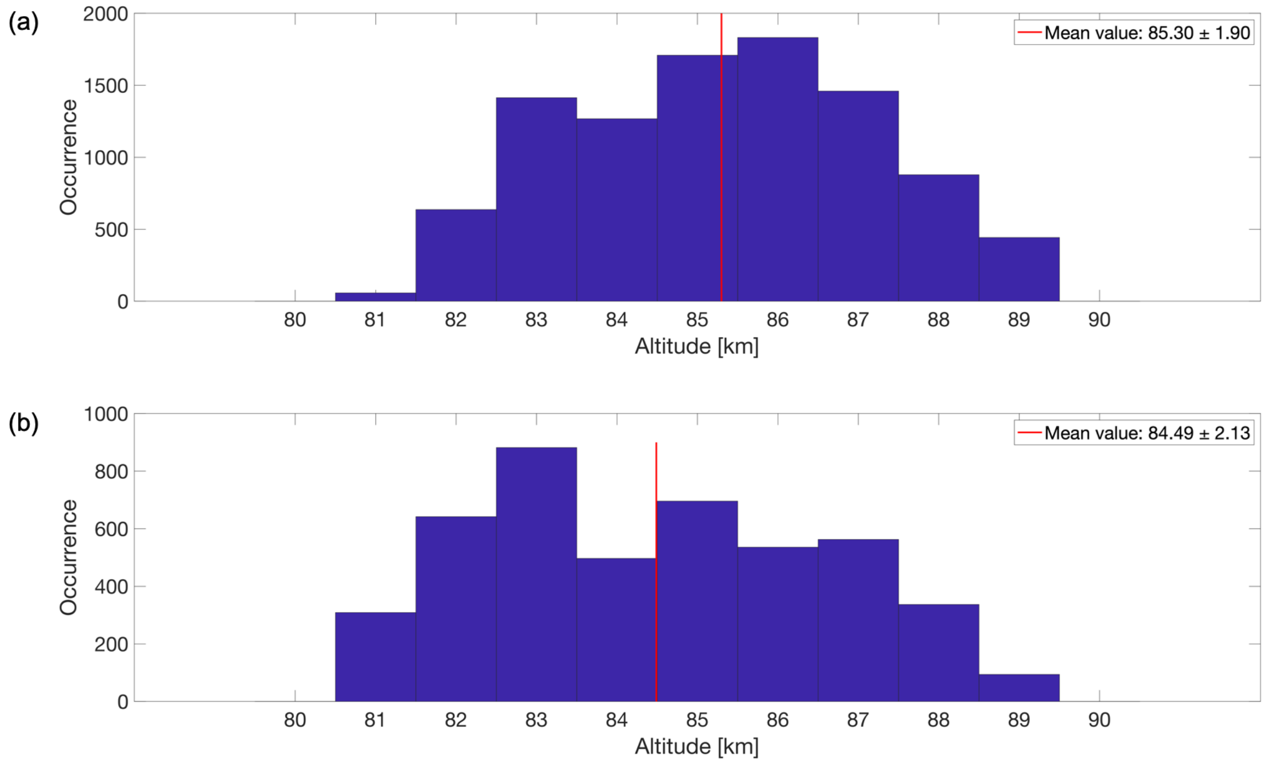

Figure 3. Altitude distribution of the data for the **(a)** solar maximum and **(b)** solar minimum. Each subplot was its respective mean altitude represented with a red line on the graph, and specified in the legend together with one standard deviation.

During solar maximum, we observe a wider range of electron densities compared to solar minimum when PMSE are present, particularly at higher electron densities. This variation in electron densities may explain why the mean electron density at an altitude of 92 km is higher during solar maximum than solar minimum during PMSE events. Additionally, our analysis reveals that the standard deviation of electron densities decreases with increasing number of layers, with mono layers exhibiting the largest standard deviations and 4-layer systems exhibiting the smallest standard deviations, for both solar maximum and minimum conditions.

3.3 Distribution of the echo power

As discussed in Sect. 2.3 we classified the data using the classification model of Jozwicki et al. (2022) and applied a threshold to identify PMSE. Specifically, we considered all echo power values above a threshold of 10.5 electrons per cubic meter in base 10 logarithmic unit as PMSE. This explains the absence of values below 10.5 on the horizontal axis of Fig. 9, Fig. 10 and Fig. 11.

In Fig. 9, it is evident that the average echo power in PMSE is higher during solar maximum than solar minimum. We noticed a greater distribution of higher values of echo power during solar maximum as compared to solar minimum, which leads to

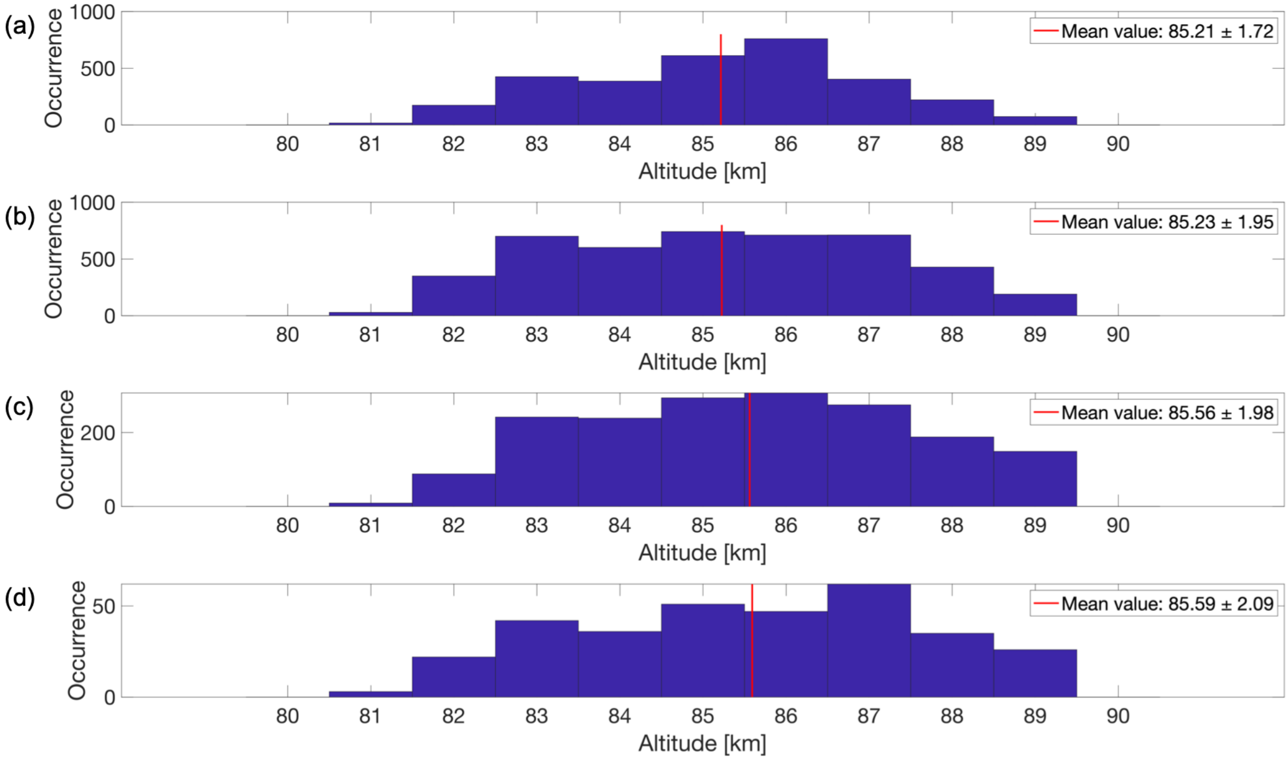

Figure 4. Altitude distribution of the data during solar maximum for **(a)** mono layers, **(b)** multi layers with 2 layers, **(c)** multi layers with 3 layers, and **(d)** multi layers with 4 layers. Each subplot was its respective mean altitude represented with a red line on the graph, and specified in the legend together with one standard deviation.

higher mean value during the solar maximum. Further, in Fig. 10, we observe that the echo power decreases as the number of multi-layers increase for solar maximum and the individual layers considered. This indicates that a single mono-layer has a higher echo power than the individual layers of two multi-layers, which in turn have a higher echo power than the individual layers of three multi-layers, and so on. However, during solar minimum as shown in Fig. 11, this trend is less evident, and we do not see a clear decrease in echo power with increasing number of layers.

3.4 Distribution of the thickness

In our study, we determined the thickness of the PMSE layers based on the number of neighboring data points, or altitude channels exceeding the echo power threshold described in Sect. 2.3. Each data point or altitude channel corresponds to a distance of 360m. As shown in Fig. 12, the average thickness of the layers is higher during solar maximum, with an average of 4.42 altitude intervals (1591m), compared to solar minimum, where the average thickness is 3.67 altitude intervals (1321m). When we examine the mono and multi-layer cases in more detail, as shown in Fig. 13 and Fig. 14, we observe that the average thickness decreases as the number of layers increases. This means that a mono-layer will be thicker than a layer belonging to

https://doi.org/10.5194/egusphere-2023-977
Preprint. Discussion started: 1 June 2023

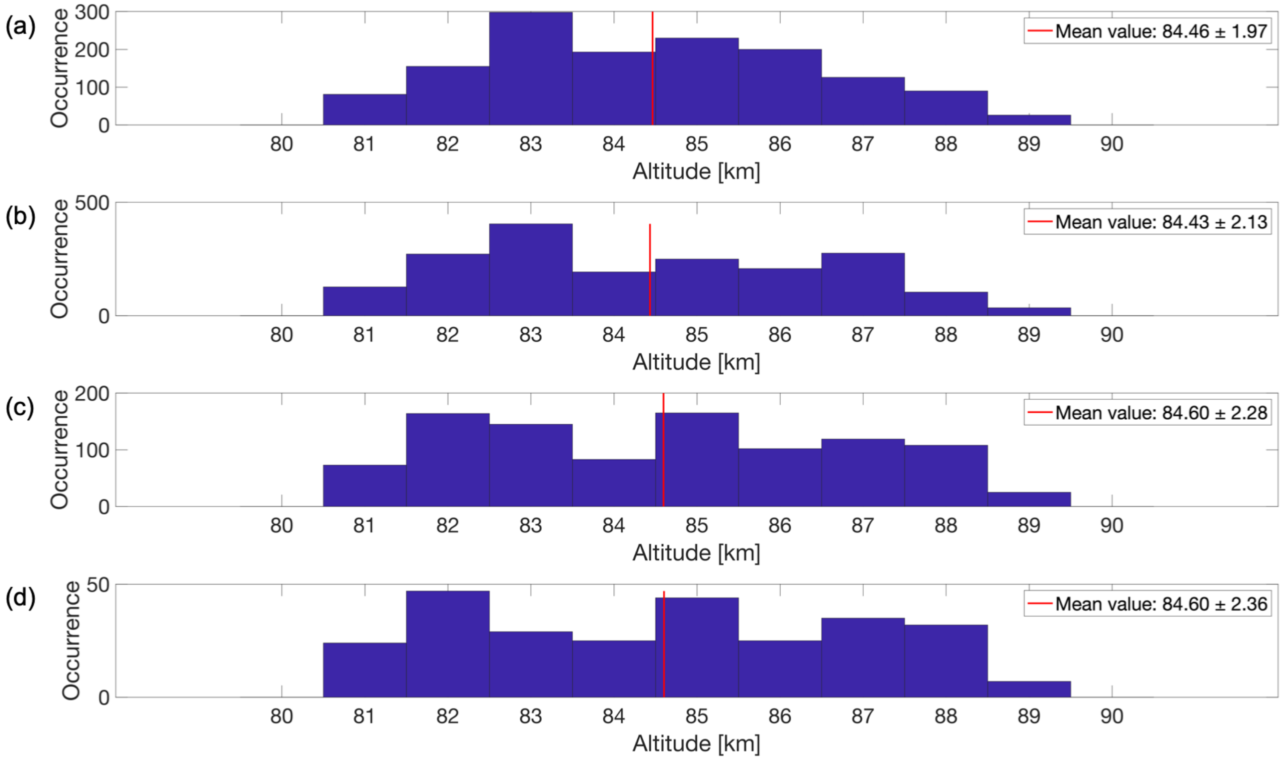

Figure 5. Altitude distribution of the data during solar minimum for **(a)** mono layers, **(b)** multi layers with 2 layers, **(c)** multi layers with 3 layers, and **(d)** multi layers with 4 layers. Each subplot was its respective mean altitude represented with a red line on the graph, and specified in the legend together with one standard deviation.

a set of 2 multi-layers, which in turn will be thicker than a layer in a 3 multi-layer case, and so on. The highest average layer thickness is obtained during solar maximum for mono-layers with an average of 5.98 data points (2153m), while the lowest average of 2.41 data points (868m) is obtained during solar minimum, for 4 multi-layers.

A compelling comparison can be drawn between the thickness of NLCs and PMSEs. Although the formation mechanisms of these two phenomena differ, there is a shared population of ice particles that contribute to both. Therefore, it is worthwhile to explore the potential similarities and differences between them. Schäfer et al. (2020) analyzed 182 hours of LIDAR data and found that NLCs occur more than half of the time (57.2%), in thick layers of more than 1 km. In our study, we analyzed 7790 instances of PMSEs with 3 or more altitude channels. Knowing that one altitude channel corresponds to 360m, 3 altitude channels or more indicate a PMSE thickness of at least 1080m. Our findings show that 54.64 percent of PMSE occurrences resulted in thick layers of 1080m or more. These results are consistent with those of Schäfer et al. (2020), where they reported that 57.2 percent of NLC occurrences were observed in thick layers of 1km or more. Additionally, Schäfer et al. (2020) classified the NLCs they observed into 10 subcategories and found that the most frequently occurring subcategory consists of thick layers composed of multiple multi-layers, with an occurrence rate of 20.5%. If we consider all types of multi layers,

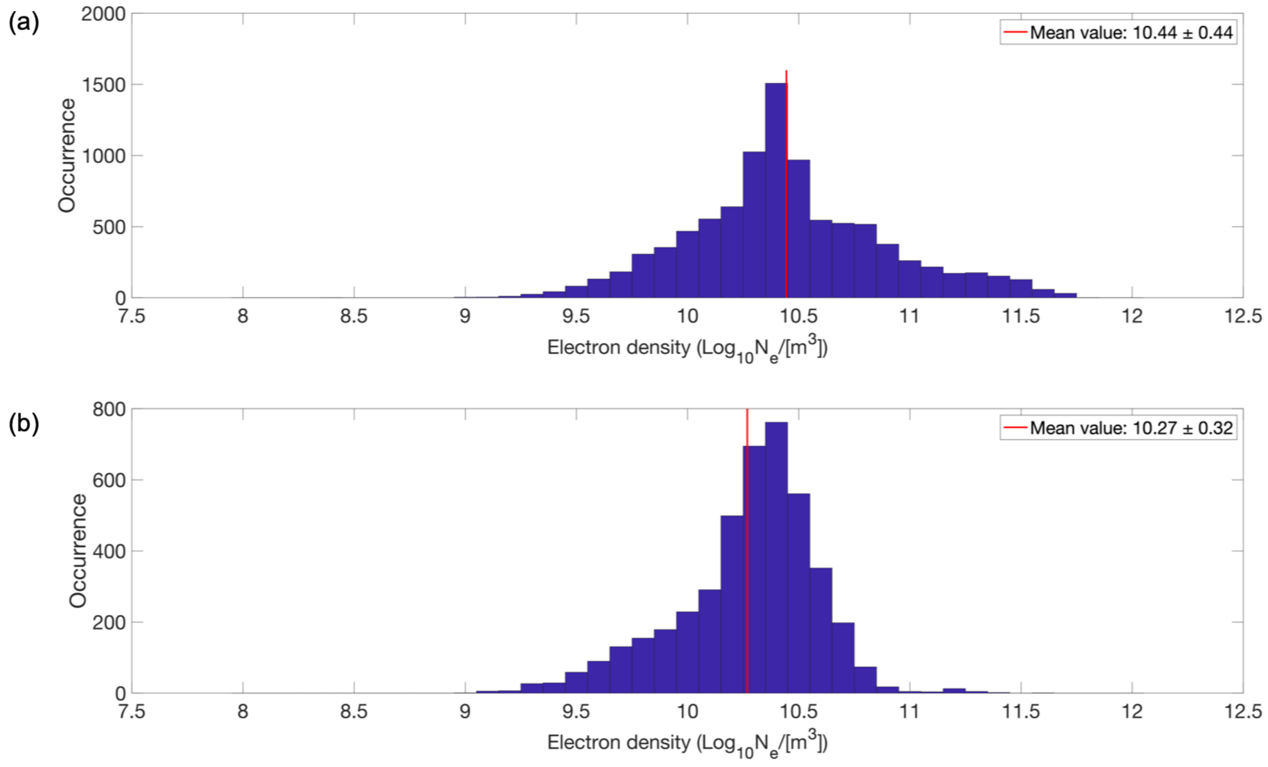

Figure 6. Electron densities at 92 km altitude for all layers during **(a)** solar maximum and **(b)** solar minimum. Each subplot was its respective mean electron density represented with a red line on the graph, and specified in the legend together with one standard deviation.

mentioned by Schäfer et al. (2020), this percentage increases up to 27.6%. In our study, multi layers happen half of the time, with an approximate occurrence rate of 49%. Therefore our results differ from the ones of Schäfer et al. (2020) when it comes to the occurrence rate of multi layers, which may be explained by some of the differences in the formation and measurement of the two phenomena.

Gravity waves are thought to play a significant role in the formation of PMSE by generating neutral turbulence in the mesosphere. The neutral turbulence caused by the gravity waves can lead to small-scale variations in the electron density, which can create the conditions necessary for PMSE to form, Rapp and Lübken (2004). Therefore, understanding the characteristics of gravity waves and their effects on the neutral atmosphere is essential for understanding the formation of PMSE. Li et al. (2016) developed a 2D theoretical model to explore the creation process of multi layered PMSE. The aim of the proposed model was to consider how gravity waves cause movement of ice particles through collisions with the neutral atmosphere. The ice particles are considered to be spherical, and their size does not vary during the simulations. This means that processes such as growth, sedimentation or sublimation are not taken into account in this model. In their first experiment, Li et al. (2016) fixed the particle size at 10 nanometers (nm) and varied the vertical wavelength of gravity waves to 3km, 4km, and 5km. They observed a decrease in the number of layers as the vertical wavelength increased. Also, the thickness of the layers increased

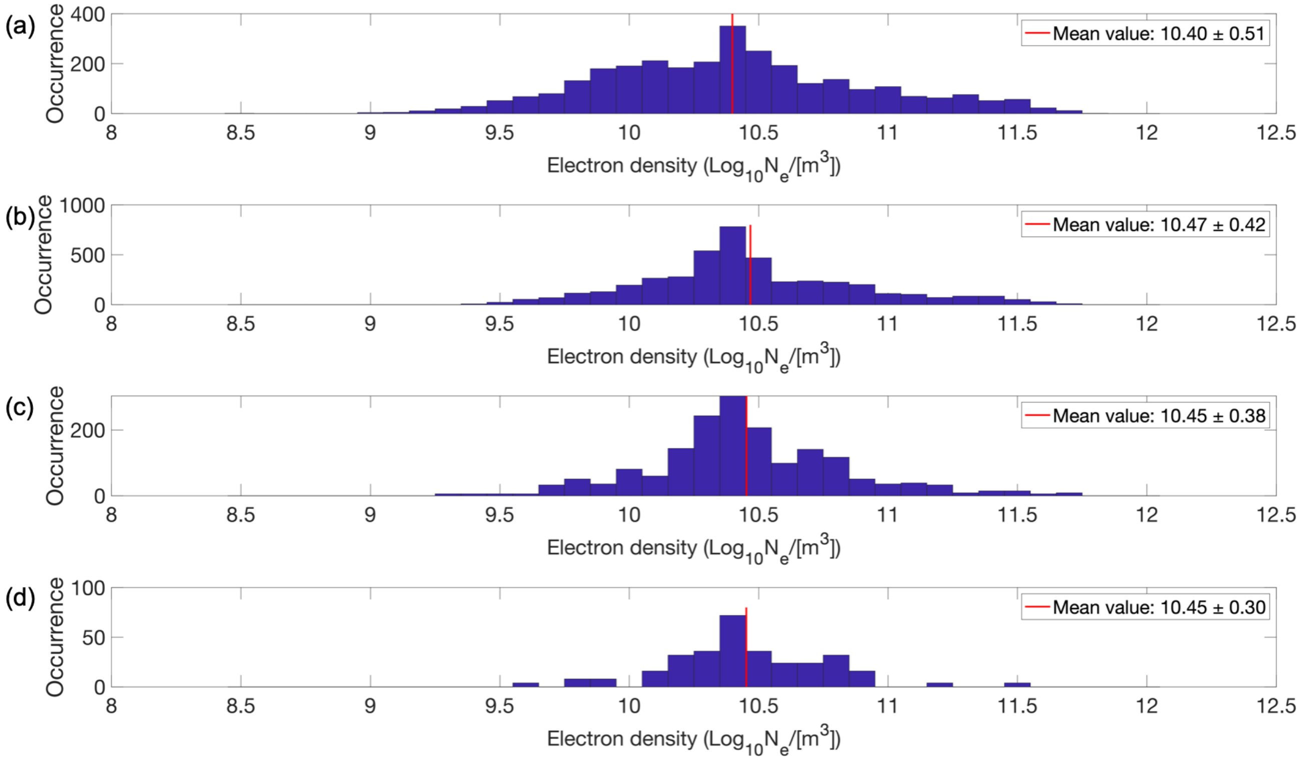

Figure 7. Electron density at 92 km altitude during solar maximum for **(a)** mono layers, **(b)** multi layers with 2 layers, **(c)** multi layers with 3 layers, and **(d)** multi layers with 4 layers. Each subplot was its respective mean electron density represented with a red line on the graph, and specified in the legend together with one standard deviation.

as the number of layers decreased. Our results on thickness distribution as shown in Fig. 12, Fig. 13 and Fig. 14 show similar trends. We found that the average thickness of mono layers was higher than that of multi layers, and the thickness decreased with an increasing number of multi layers. One possible hypothesis that can be drawn is that the thickness of the layers could be related to the vertical wavelength of gravity waves, with higher wavelengths producing thicker layers.

Li et al. (2016) reported the observation of preferred altitudes for each multi layer formation, which depended on the size of the ice particles. One might expect to observe distinct peaks in the distribution of multi layers for each size range. A plausible hypothesis is that if such peaks are not observed, and instead a more uniform distribution is seen, this could be due to the presence of ice particles of various sizes that create peaks at different altitudes, resulting in a smoothed-out distribution. In Fig. 5, which shows the altitude distribution for mono and multi layers during solar minimum, the distributions appear less smooth than those in Fig. 4. This observation could support the hypothesis that the range of size distributions of ice particles is smaller during solar minimum as compared to solar maximum. Potential mechanisms for ice formation at upper mesospheric altitudes that could be affected by the solar cycle are unknown to the authors, but this is something to investigate in a future study. In another experiment in Li et al. (2016) study investigated the effect of varying ice particle size while fixing the vertical

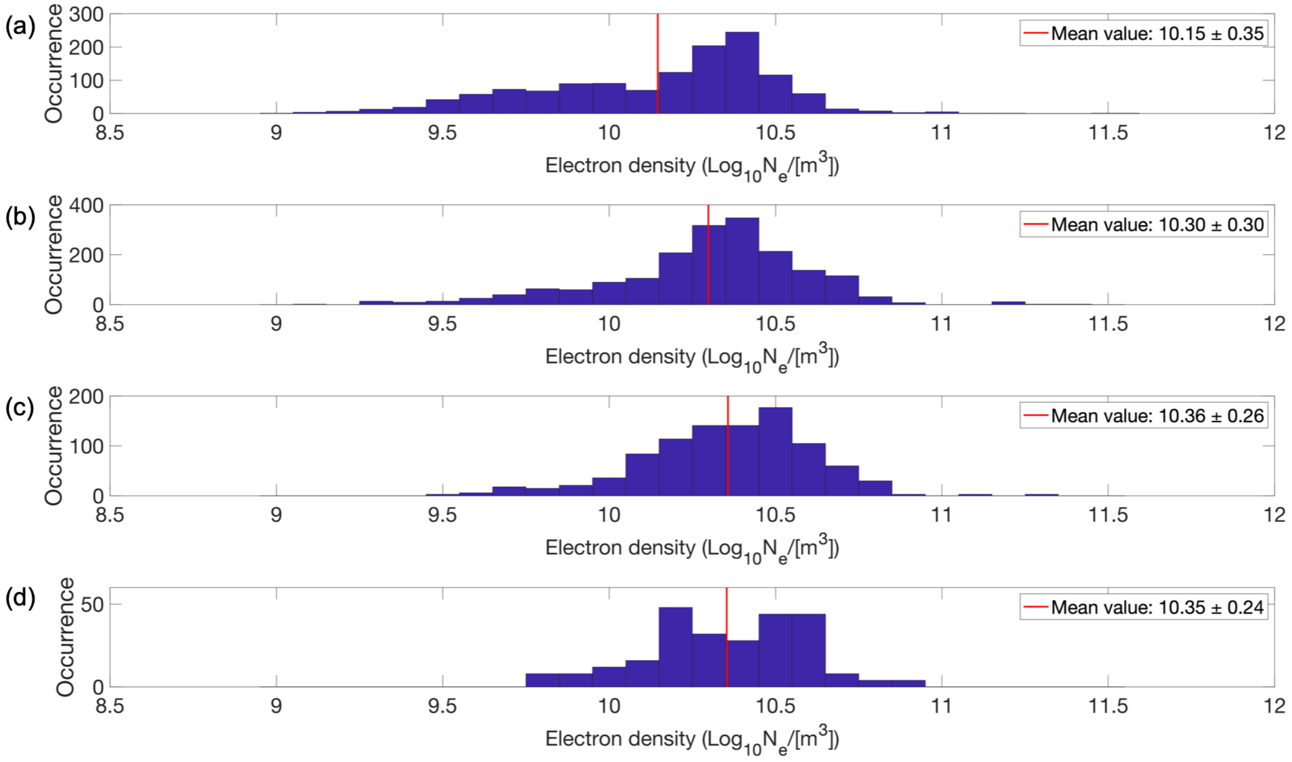

Figure 8. Electron density at 92 km altitude during solar minimum for **(a)** mono layers, **(b)** multi layers with 2 layers, **(c)** multi layers with 3 layers, and **(d)** multi layers with 4 layers. Each subplot was its respective mean electron density represented with a red line on the graph, and specified in the legend together with one standard deviation.

wavelength of gravity waves at 4km. They used particle sizes of 10nm, 20nm, and 30nm and found that the altitude of the layers decreased more rapidly and their formation became more challenging with increasing particle size. Also, once the turbulence stopped, the larger ice particles took longer to go back to a neutral homogeneous state. It is worth noting that their model does not consider the growth, sedimentation, and sublimation processes, so these findings should be considered as preliminary hypotheses.

In their study, Singer et al. (2012) observed the intensification of westward winds below 85 km and eastward winds above 85 km during the summer season. They also noted that gravity waves with periods of 3 to 6 hours, between 80 km and 88 km, are more active at an altitude of about 75 km. Additionally, they found that severe solar proton events result in an increase in eastward winds above 85 km. These wind and gravity wave behaviors at PMSE altitudes might be the key factors in understanding the turbulence leading to multi-layered PMSE formation.

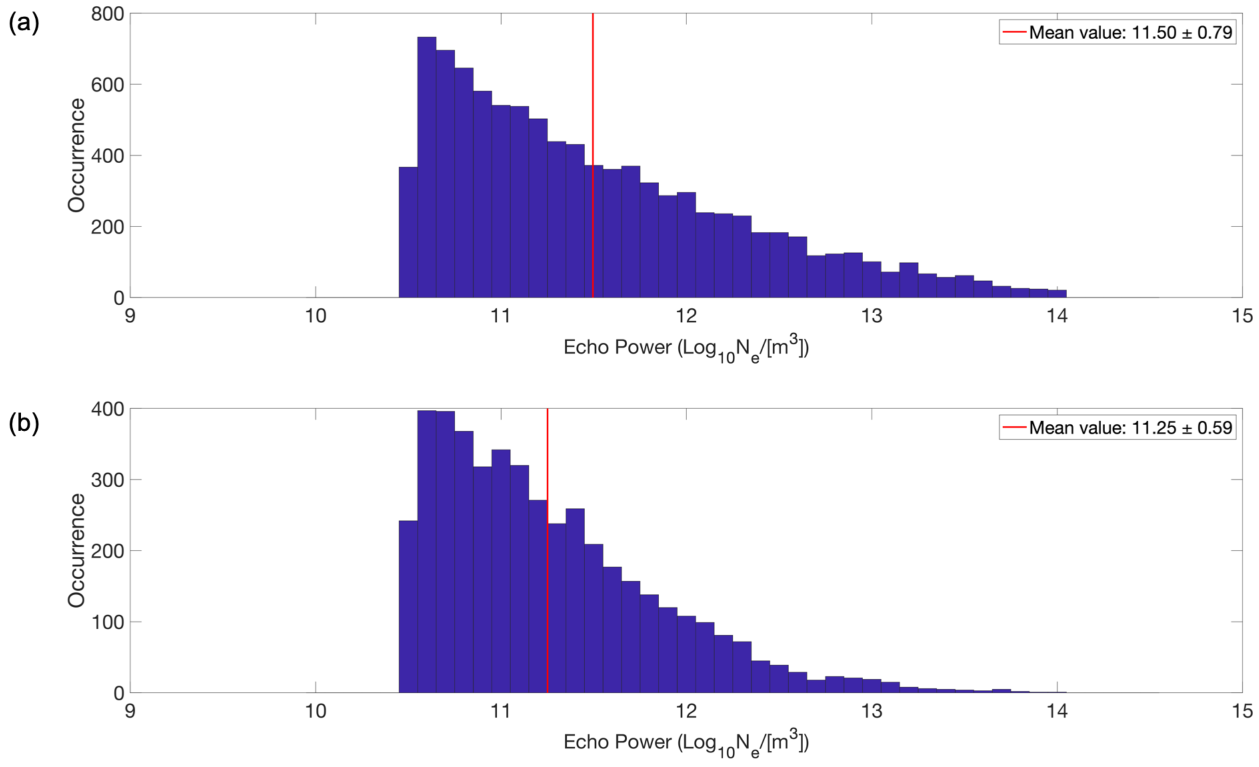

Figure 9. Echo power in the PMSE for all layers during **(a)** solar maximum and **(b)** solar minimum. Each subplot has its respective mean echo power represented with a red line on the graph, and specified in the legend together with one standard deviation.

3.5 Correlations

In this section, we will analyze the correlation between several parameters, namely electron density, echo power, thickness, and altitude. Table 3 shows both correlation coefficients for all layers together, for the solar maximum on the lower portion of the table, and for the solar minimum on the upper portion of the table. Table 4(a) shows the results of the Pearson correlation coefficient only, for mono and multi layers separately, and for solar maximum and minimum. Table 4(b) shows the results of the Spearman's rank correlation coefficient only, for mono and multi layers separately, and for solar maximum and minimum. For simplicity, in all the mentioned above tables, the notation "r_p" is chosen to represent Pearson correlation coefficients, and the notation "r_s" is chosen to represent Spearman's rank correlation coefficients. In Tables 4(a) and 4(b), the notations "r_{p1}", "r_{p2}", "r_{p3}" and "r_{p4}" denote the Pearson correlation coefficients for mono layers, double layers, triple layers, and quadruple layers respectively. In a similar manner, the Spearman's rank correlation coefficient notations are "r_{s1}", "r_{s2}", "r_{s3}" and "r_{s4}".

In Table 3, it is observed that the electron density at 92 km altitude and the echo power are positively correlated with the thickness of all the layers for both solar maximum and solar minimum. This is also the case for Tables 4(a), and 4(b). During solar maximum, the positive correlation between electron density and thickness is greater than during solar minimum, but

https://doi.org/10.5194/egusphere-2023-977
Preprint. Discussion started: 1 June 2023

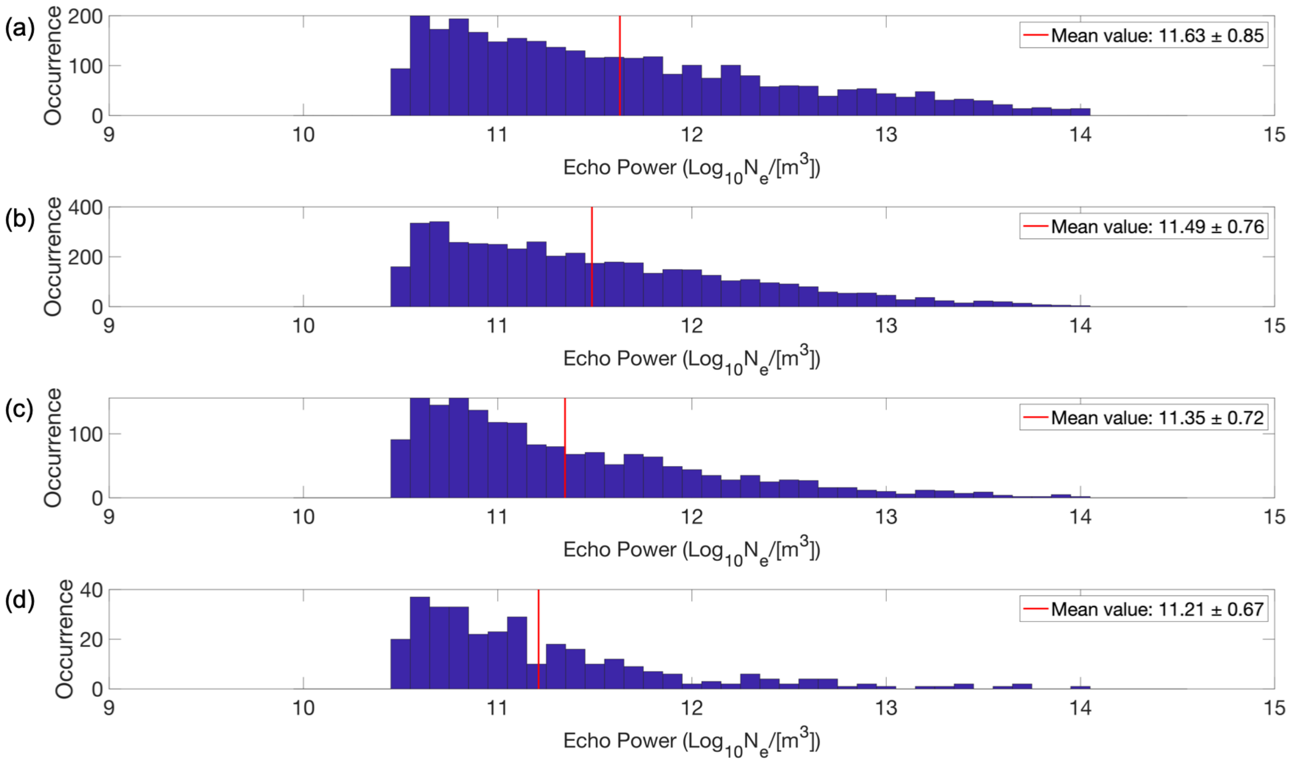

Figure 10. Echo power in the PMSE during solar maximum for **(a)** mono layers, **(b)** multi layers with 2 layers, **(c)** multi layers with 3 layers, and **(d)** multi layers with 4 layers. Each subplot has its respective mean echo power represented with a red line on the graph, and specified in the legend together with one standard deviation.

Table 3. Pearson and Spearman's rank correlation coefficients for all layers together, for solar maximum and solar minimum.

		Solar minimum			
		Electron density	Echo power	Thickness	Altitude
Solar maximum	Electron density		$r_p = 0.213$ $r_s = 0.163$	$r_p = 0.251$ $r_s = 0.232$	$r_p = -0.079$ $r_s = -0.058$
	Echo power	$r_p = 0.338$ $r_s = 0.305$		$r_p = 0.521$ $r_s = 0.631$	$r_p = -0.165$ $r_s = -0.162$
	Thickness	$r_p = 0.480$ $r_s = 0.392$	$r_p = 0.510$ $r_s = 0.631$		$r_p = -0.153$ $r_s = -0.169$
	Altitude	$r_p = 0.011$ $r_s = 0.003$	$r_p = -0.034$ $r_s = -0.031$	$r_p = 0.039$ $r_s = 0.024$	

Table 4. (a) Pearson correlation coefficients for mono and multi layers separately, for solar maximum and solar minimum. **(b)** Spearman's rank correlation coefficients for mono and multi layers separately, for solar maximum and solar minimum.

(a)		Solar minimum			
		Electron density	Echo power	Thickness	Altitude
Solar maximum	Electon density		$\mathrm{r}_{p1} = 0.270$ $\mathrm{r}_{p2} = 0.247$ $\mathrm{r}_{p3} = 0.163$ $\mathrm{r}_{p4} = 0.199$	$\mathrm{r}_{p1} = 0.376$ $\mathrm{r}_{p2} = 0.273$ $\mathrm{r}_{p3} = 0.226$ $\mathrm{r}_{p4} = 0.168$	$\mathrm{r}_{p1} = -0.339$ $\mathrm{r}_{p2} = 0.010$ $\mathrm{r}_{p3} = 0.048$ $\mathrm{r}_{p4} = 0.054$
	Echo power	$\mathrm{r}_{p1} = 0.501$ $\mathrm{r}_{p2} = 0.259$ $\mathrm{r}_{p3} = 0.224$ $\mathrm{r}_{p4} = 0.306$		$\mathrm{r}_{p1} = 0.455$ $\mathrm{r}_{p2} = 0.574$ $\mathrm{r}_{p3} = 0.608$ $\mathrm{r}_{p4} = 0.514$	$\mathrm{r}_{p1} = -0.071$ $\mathrm{r}_{p2} = -0.186$ $\mathrm{r}_{p3} = -0.228$ $\mathrm{r}_{p4} = -0.210$
	Thickness	$\mathrm{r}_{p1} = 0.695$ $\mathrm{r}_{p2} = 0.393$ $\mathrm{r}_{p3} = 0.246$ $\mathrm{r}_{p4} = 0.264$	$\mathrm{r}_{p1} = 0.534$ $\mathrm{r}_{p2} = 0.482$ $\mathrm{r}_{p3} = 0.508$ $\mathrm{r}_{p4} = 0.541$		$\mathrm{r}_{p1} = -0.110$ $\mathrm{r}_{p2} = -0.199$ $\mathrm{r}_{p3} = -0.167$ $\mathrm{r}_{p4} = -0.161$
	Altitude	$\mathrm{r}_{p1} = 0.091$ $\mathrm{r}_{p2} = -0.079$ $\mathrm{r}_{p3} = -0.046$ $\mathrm{r}_{p4} = 0.030$	$\mathrm{r}_{p1} = 0.087$ $\mathrm{r}_{p2} = -0.052$ $\mathrm{r}_{p3} = -0.118$ $\mathrm{r}_{p4} = -0.184$	$\mathrm{r}_{p1} = 0.131$ $\mathrm{r}_{p2} = 0.031$ $\mathrm{r}_{p3} = -0.040$ $\mathrm{r}_{p4} = -0.113$	

(b)		Solar minimum			
		Electron density	Echo power	Thickness	Altitude
Solar maximum	Electron density		$r_{s1} = 0.245$ $r_{s2} = 0.179$ $r_{s3} = 0.178$ $r_{s4} = 0.123$	$r_{s1} = 0.428$ $r_{s2} = 0.215$ $r_{s3} = 0.178$ $r_{s4} = 0.173$	$r_{s1} = -0.292$ $r_{s2} = 0.006$ $r_{s3} = 0.045$ $r_{s4} = 0.047$
	Echo power	$r_{s1} = 0.494$ $r_{s2} = 0.239$ $r_{s3} = 0.202$ $r_{s4} = 0.232$		$r_{s1} = 0.603$ $r_{s2} = 0.643$ $r_{s3} = 0.635$ $r_{s4} = 0.542$	$r_{s1} = -0.047$ $r_{s2} = -0.188$ $r_{s3} = -0.240$ $r_{s4} = -0.208$
	Thickness	$r_{s1} = 0.668$ $r_{s2} = 0.311$ $r_{s3} = 0.202$ $r_{s4} = 0.230$	$r_{s1} = 0.615$ $r_{s2} = 0.621$ $r_{s3} = 0.637$ $r_{s4} = 0.595$		$r_{s1} = -0.168$ $r_{s2} = -0.185$ $r_{s3} = -0.141$ $r_{s4} = -0.124$
	Altitude	$r_{s1} = 0.095$ $r_{s2} = -0.052$ $r_{s3} = -0.031$ $r_{s4} = 0.058$	$r_{s1} = 0.111$ $r_{s2} = -0.051$ $r_{s3} = -0.107$ $r_{s4} = -0.190$	$r_{s1} = 0.161$ $r_{s2} = 0.008$ $r_{s3} = -0.052$ $r_{s4} = -0.076$	

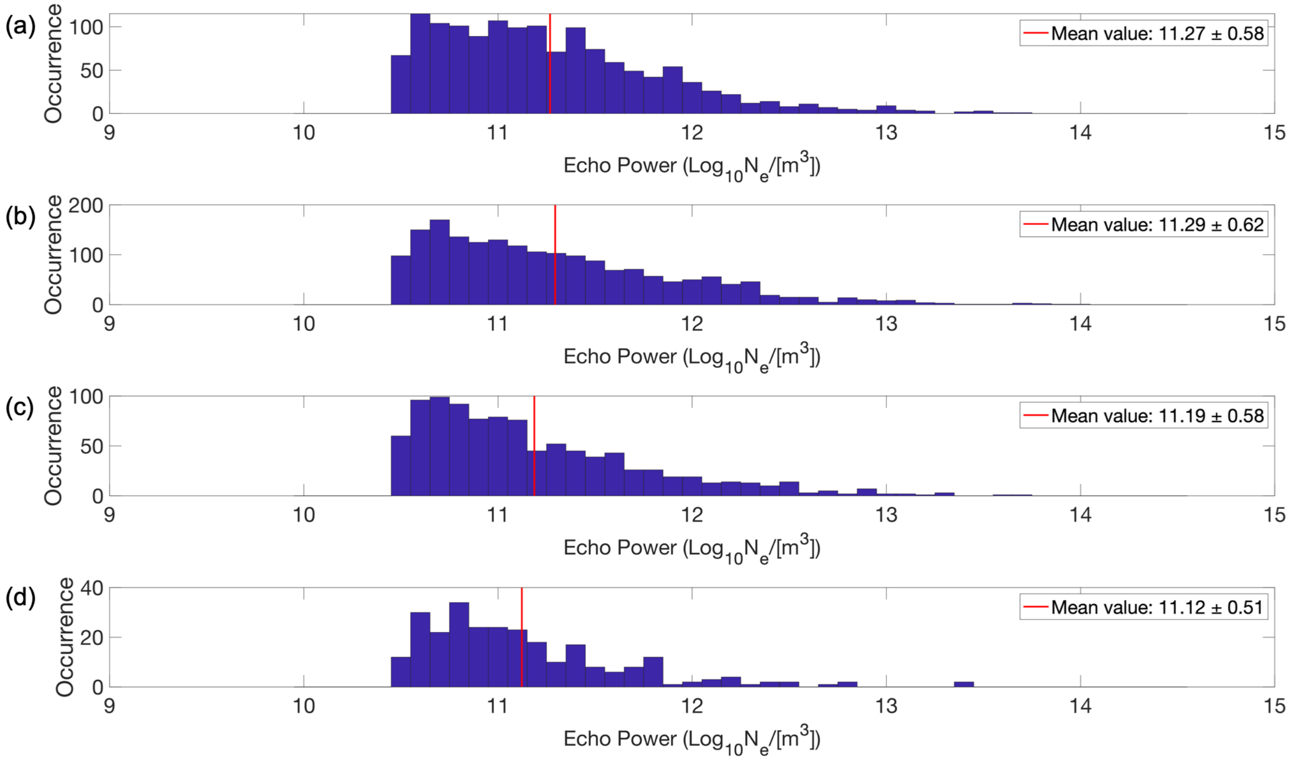

Figure 11. Echo power in the PMSE during solar minimum for **(a)** mono layers, **(b)** multi layers with 2 layers, **(c)** multi layers with 3 layers, and **(d)** multi layers with 4 layers. Each subplot has its respective mean echo power represented with a red line on the graph, and specified in the legend together with one standard deviation.

this is not observed between echo power and thickness. In Tables 3, the Pearson correlation coefficient of 0.480 for solar maximum suggests a moderate positive linear relationship between electron density and thickness, while the Spearman's rank correlation coefficient of 0.392 indicates a moderate positive monotonic relationship between the variables for the same case. Since the two values are similar, it suggests that during solar maximum there is a consistent association between electron density and thickness. In Tables 4(a), and 4(b), we observe that the Pearson correlation coefficient and Spearman's rank correlation coefficient between electron density and thickness decrease as the number of multi layers increases. Specifically, in both cases the highest correlation is observed for solar maximum and mono layers, with a Pearson coefficient of 0.695 and a Spearman's rank coefficient of 0.668. This could possibly indicate that at higher ionization levels at this altitude, the PMSE mono layers are thicker. Conversely, the lowest correlations were obtained for solar minimum and the largest number of multi layers, which is 4, with a Pearson coefficient of 0.168 and a Spearman's rank coefficient of 0.173.

From Tables 3, 4(a), and 4(b) we notice a weak negative correlation between the echo power in the PMSE and altitude for all layers during both solar maximum and solar minimum. The strongest negative correlation is found for 3 multi layers, with a Pearson coefficient of -0.228 and a Spearman's rank coefficient of -0.240. Notably, altitude appears to be uncorrelated with the

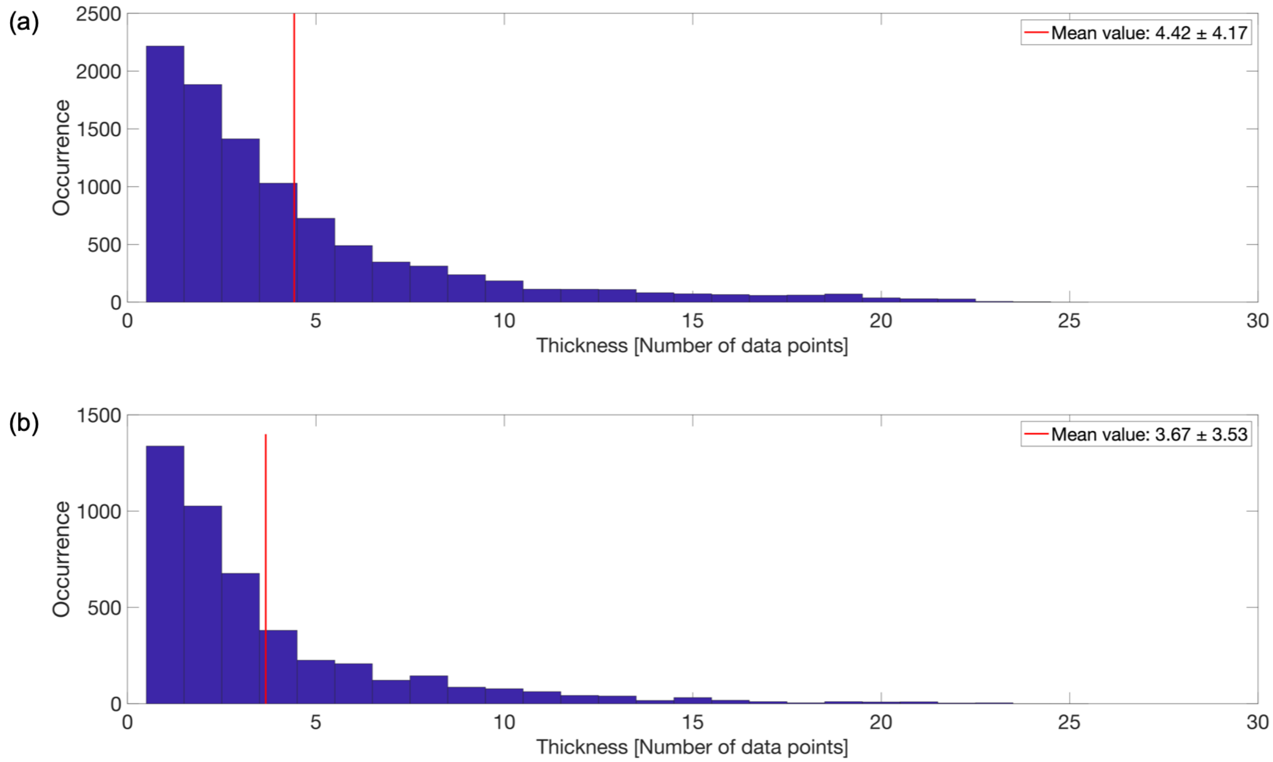

Figure 12. Thickness distribution of the layers for all layers combined during **(a)** solar maximum and **(b)** solar minimum. Each subplot was its respective mean thickness represented with a red line on the graph, and specified in the legend together with one standard deviation.

other variables, implying that additional factors may be influencing the formation of PMSE at specific altitudes. For example, this could be attributed to mesopause conditions, gravity wave wavelength and ice particle size.

From Tables 3, 4(a), and 4(b) we notice overall the positive correlation between the electron density at 92 km altitude and the echo power in the PMSE for all the layers and for both solar maximum and solar minimum. For Tables 4(a) and 4(b), we note that the highest Pearson correlation coefficient and Spearman's rank correlation coefficient are obtained for mono layers. Specifically for solar maximum, the Pearson coefficient is 0.501 and the Spearman's rank coefficient is 0.494, while for solar minimum, the Pearson coefficient is 0.270 and the Spearman's rank coefficient is 0.245. These results can possibly suggest that at higher ionization levels at 92 km altitude, the PMSE have a higher intensity, indicated by a higher echo power, particularly in the case of mono layers during solar maximum. On the other hand, the lowest correlations were found for multi layers containing three layers, with a Pearson coefficient of 0.224 and a Spearman's rank coefficient of 0.202 for solar maximum and a Pearson coefficient of 0.306 and a Spearman's rank coefficient of 0.232 for solar minimum.

In their study, Narayanan et al. (2022) found that there was a clear response in the power of the PMSE echoes during particle precipitation events: in all their cases, an increase in PMSE power was observed in association with particle precipitations. However, Narayanan et al. (2022) say that the particle precipitation does not seem to be related to the very existence of PMSE,

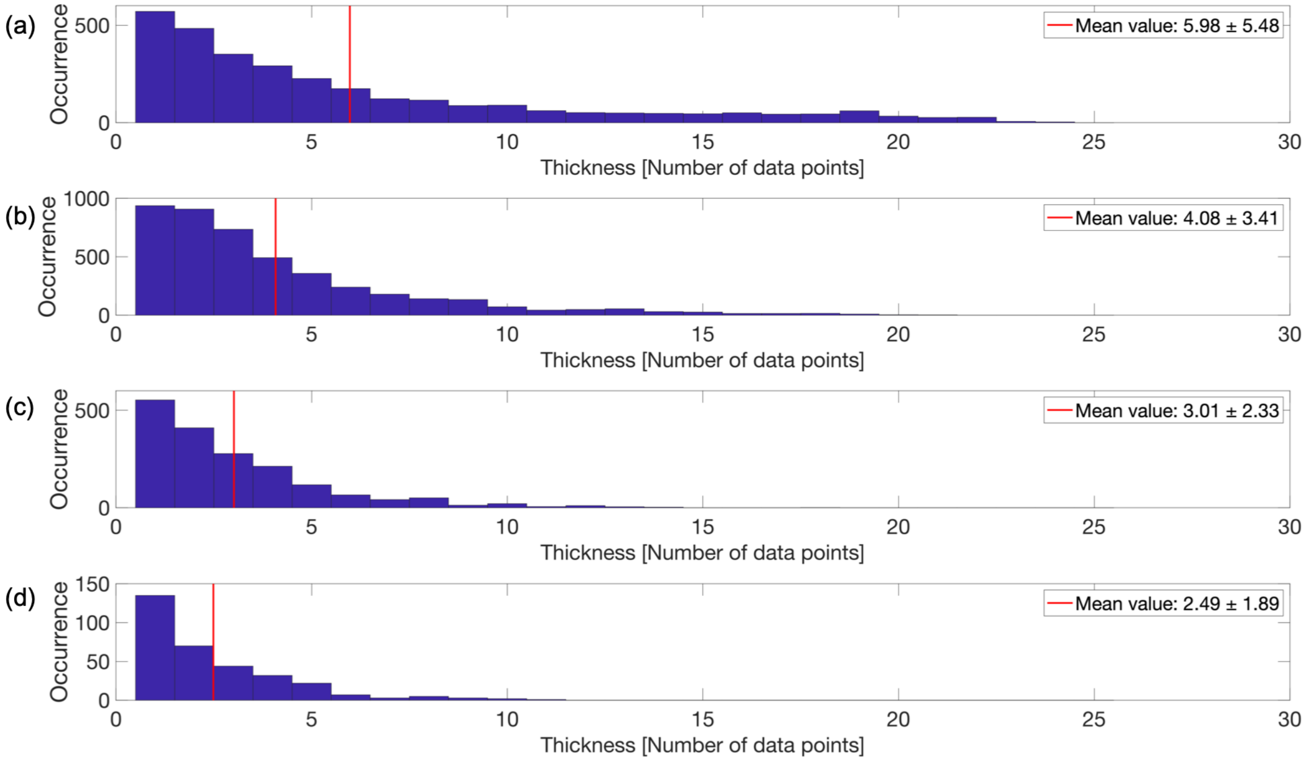

Figure 13. Thickness distribution during solar maximum for **(a)** mono layers, **(b)** multi layers with 2 layers, **(c)** multi layers with 3 layers, and **(d)** multi layers with 4 layers. Each subplot was its respective mean thickness represented with a red line on the graph, and specified in the legend together with one standard deviation.

and that there seem to be no linear relationship between both, which is consistent with the results of our study. Specifically, we observe weak Pearson correlation coefficients during the solar minimum, as reported in Table 4(a), consistent with the findings of Narayanan et al. (2022) who analyzed EISCAT VHF observations from 2019, a period corresponding to the solar minimum. However, our results indicate slightly higher Pearson correlation coefficients during solar maximum, particularly for mono layers. It would be worthwhile to conduct a similar investigation as Narayanan et al. (2022) during the solar maximum phase of a solar cycle. These findings should be interpreted with care, considering that our study differs from that of Narayanan et al. (2022) in several ways. Specifically, our data selection process did not require the simultaneous presence of PMSE and particle precipitation.

From Table 3, one can notice that for the combination of echo power and electron density during solar maximum, the obtained Pearson correlation coefficient is 0.338 and the Spearman's rank correlation coefficient is 0.305. In their study, Rauf et al. (2018a) used EISCAT VHF data to investigate the correlation between PMSE strength and particle precipitation, over a dataset of 111 hours, or 5 days of observation. However in their case, they derived the Pearson and Spearman correlation coefficients between their PMSE proxy which is equivalent to our use of the term "echo power", and the electron density at 90

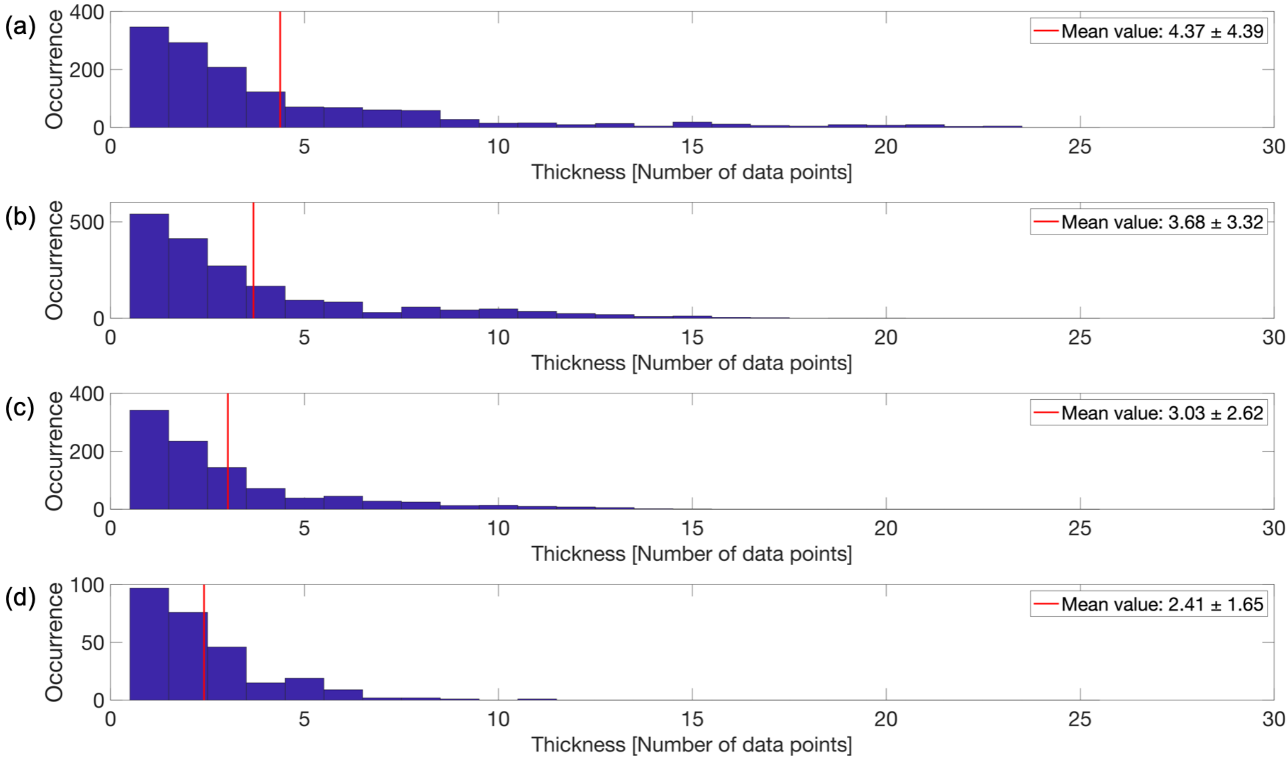

Figure 14. Thickness distribution during solar minimum for **(a)** mono layers, **(b)** multi layers with 2 layers, **(c)** multi layers with 3 layers, and **(d)** multi layers with 4 layers. Each subplot was its respective mean thickness represented with a red line on the graph, and specified in the legend together with one standard deviation.

km altitude instead of 92 km for us. Nevertheless, it is interesting to note that they also found a positive correlation between echo power and electron density with 0.15 for the Pearson correlation coefficient, and 0.24 for the Spearman correlation coefficient. It is important to note that during their analysis, Rauf et al. (2018a) only selected data from 8 to 12 July 2013, when PMSE and particle precipitation were occurring simultaneously. The year 2013 is included in our study in the solar maximum data, therefore we compare Rauf et al. (2018a) correlation coefficients with our correlation coefficients for solar maximum. In our study, we included data from the year 2013 in the solar maximum period. Hence, we compare the correlation coefficients from Rauf et al. (2018a) with our own coefficients for the solar maximum. While both studies discovered a positive correlation, our findings had higher correlation coefficients than Rauf et al. (2018a) study. One factor which could explain this difference might be the fact that in Rauf et al. (2018a) data, PMSE and particle precipitation was always occurring simultaneously, while in our analysis, data was selected solely based on the presence of PMSE, without any filtering based on the occurrence of particle precipitation. It should be noted that while PMSE was present in all of our cases, there may have been instances where particle precipitation was present and instances where it was not. Another factor might be that we used a lower threshold for PMSE

https://doi.org/10.5194/egusphere-2023-977
Preprint. Discussion started: 1 June 2023

detection than Rauf et al. (2018a), due to the fact that we used a classification model on the data before hand. We used the threshold $N_e > 3.2 \times 10^{10} m^{-3}$ while Rauf et al. (2018a) used $N_e > 4.6 \times 10^{11} m^{-3}$.

4 Conclusions

The results from our study indicate that the altitude, the echo power and the thickness of layers in PMSE have on average higher values during solar maximum than during solar minimum. As expected, the electron density at 92 km is on average higher during solar maximum than solar minimum. Based on our investigation, we have found that the electron density at 92 km altitude and the echo power are positively correlated with the thickness for all the layers and for both solar maximum and solar minimum. The echo power and electron density are positively correlated, especially for mono layers and solar maximum. This can possibly suggest that under those conditions and at higher ionization levels at 92 km altitude, the PMSE are stronger, indicated by a higher echo power. For both solar maximum and solar minimum periods, the mono layers attained the lowest average electron density of their respective seasons, though the trend was relatively weak. A plausible argument could be made that higher electron densities at ionospheric altitudes might be necessary to generate multi-layered PMSEs. The electron density was also highly correlated with the thickness of the layers especially for solar maximum and mono layers, which indicates that at higher ionization levels at 92km altitude, the PMSE mono layers are commonly thicker.

The echo power was found to decrease with increasing multi layers, but only in the case of solar maximum. Furthermore, we have observed that the thickness decreases as the number of multi-layers increases, indicating that a single mono-layer will be thicker than the separate layers of a set of two multi-layers, which in turn will be thicker than the separate layers of three multi-layers, and so on. This suggests that there may be a relationship between the number of layers, echo power, and thickness. Our study is consistent with the findings of Li et al. (2016) where they found that the thickness of multi layers decreases with increasing number of multi layers. Comparing our results with Li et al. (2016) led us to hypothesize that the thickness of the layers could be related to the vertical wavelength of gravity waves, with larger wavelengths producing thicker layers. Further investigations could explore this hypothesis, potentially providing a means to infer the wavelength of gravity waves through PMSE observations at these altitudes.

Our study is consistent with previous research from Hoffmann et al. (2005) regarding the altitude of the observed mono layers and the occurence rate of PMSE mono and multi layers. We also found similar results as Rauf et al. (2018a), discovering a positive correlation between electron density and echo power. Taking into account the findings presented by Lübken et al. (2021) that show an increase in ice particle size over time, and in conjunction with our own results, it is possible to hypothesize that factors other than the sole influence from the solar cycle might play a significant role in the altitude of PMSEs. An interesting parallel could be drawn with the findings of Schäfer et al. (2020) regarding multi layered NLC, where both our studies found a similar occurrence rate for thick layer formation above 1 km thickness. In light of the similarities in multi-layer formation between PMSE and NLC, future studies may be able to utilize findings from NLC research to gain insights into PMSE dynamics.

The altitude region where PMSE form is a site of significant activity and dynamics. As we discussed in the previous section, other factors besides the sole influence of the solar cycle play an important role in multi-layer PMSE formation. Singer et al. (2012) study highlights the significant activity that occurs within the PMSE height range. As a suggestion for future research, it would be worth investigating the connections between multi-layered PMSE formation and winds and gravity waves rather than solely focusing on the solar cycle.

In conclusion, the mechanism of the formation PMSE might be presently well understood, however the exact conditions leading to multi-layered PMSE formation remains unclear, and further investigation is required. Understanding the complex interplay of the factors involving the formation of PMSE is crucial to gain insights into the thermodynamic and fluid dynamic processes occurring at altitudes between 80 to 90 km. We have provided evidence of PMSE properties being potentially related to gravity wave vertical wavelength, ice particle size, and electron density.

Data availability. EISCAT VHF data are available under http://www.eiscat.se/madrigal/ (accessed on 15 January 2023).

Author contributions. Conceptualization, D.J., P.S., D.H. and I.M.; Data curation, D.J.; Funding acquisition, I.M.; Investigation, D.J.; Project administration, I.M.; Software, D.J.; Supervision, P.S., D.H. and I.M.; Validation, P.S., D.H. and I.M.; Writing—original draft, D.J.; Writing—review and editing, D.J., P.S. D.H. and I.M. All authors have read and agreed to the published version of the manuscript.

Competing interests. The authors declare no conflict of interest. The funders had no role in the design of the study; in the collection, analyses, or interpretation of data; in the writing of the manuscript, or in the decision to publish the results.

Acknowledgements. This work was carried out within a project funded by Research Council of Norway, NFR 275503. The Norwegian participation in EISCAT and EISCAT3D is funded by Research Council of Norway, through research infrastructure grant 245683. The EISCAT International Association is supported by research organizations in Norway (NFR), Sweden (VR), Finland (SA), Japan (NIPR and STEL), China (CRIPR), and the United Kingdom (NERC).

Devin Huyghebaert was funded during this study through a UiT The Arctic University of Norway contribution to the EISCAT_3D project funded by Research Council of Norway through research infrastructure grant 245683.

References

Avaste, O.: Noctilucent clouds, Journal of Atmospheric and Terrestrial Physics, 55, 133–143, https://doi.org/https://doi.org/10.1016/0021-9169(93)90118-I, 1993.

Belova, E., Chilson, P. B., Kirkwood, S., and Rietveld, M. T.: The response time of PMSE to ionospheric heating, Journal of Geophysical Research: Atmospheres, 108, https://doi.org/https://doi.org/10.1029/2002JD002385, 2003.

Beynon, W. and Williams, P.: Incoherent scatter of radio waves from the ionosphere, Reports on Progress in Physics, 41, 909–956, https://doi.org/doi:10.1088/0034-4885/41/6/003, 1978.

Cho, J. Y. N. and Röttger, J.: An updated review of polar mesosphere summer echoes: Observation, theory, and their relationship to noctilucent clouds and subvisible aerosols, , 102, 2001–2020, https://doi.org/10.1029/96JD02030, 1997.

Hocking, W., Rüster, R., and Czechowsky, P.: Absolute reflectivities and aspect sensitivities of VHF radio wave scatterers measured with the SOUSY radar, Journal of Atmospheric and Terrestrial Physics, 48, 131–144, https://doi.org/https://doi.org/10.1016/0021-9169(86)90077-2, 1986.

Hoffmann, P., Rapp, M., Serafimovich, A., and Latteck, R.: On the occurrence and formation of multiple layers of polar mesosphere summer echoes, Geophysical Research Letters, 32, https://doi.org/https://doi.org/10.1029/2004GL021409, 2005.

Jozwicki, D., Sharma, P., Mann, I., and Hoppe, U.-P.: Segmentation of PMSE Data Using Random Forests, Remote Sensing, 14, https://doi.org/10.3390/rs14132976, 2022.

Latteck, R., Renkwitz, T., and Chau, J. L.: Two decades of long-term observations of polar mesospheric echoes at 69°N, Journal of Atmospheric and Solar-Terrestrial Physics, 216, 105576, https://doi.org/10.1016/j.jastp.2021.105576, 2021.

Lehtinen, M. S. and Huuskonen, A.: General incoherent scatter analysis and GUISDAP, Journal of Atmospheric and Terrestrial Physics, 58, 435–452, https://doi.org/https://doi.org/10.1016/0021-9169(95)00047-X, selected papers from the sixth international Eiscat Workshop, 1996.

Li, H., Wu, J., and Zhou, Z.: The formation of multiple layers of ice particles in the polar summer mesopause region, Annales Geophysicae, 34, 117–122, https://doi.org/10.5194/angeo-34-117-2016, 2016.

Lübken, F.-J., Berger, U., and Baumgarten, G.: Stratospheric and solar cycle effects on long-term variability of mesospheric ice clouds, Journal of Geophysical Research: Atmospheres, 114, https://doi.org/https://doi.org/10.1029/2009JD012377, 2009.

Lübken, F.-J., Baumgarten, G., and Berger, U.: Long term trends of mesopheric ice layers: A model study, Journal of Atmospheric and Solar-Terrestrial Physics, 214, 105 378, https://doi.org/https://doi.org/10.1016/j.jastp.2020.105378, 2021.

Narayanan, V. L., Häggström, I., and Mann, I.: Effects of particle precipitation on the polar mesospheric summer echoes observed by EISCAT VHF 224 MHz radar, Advances in Space Research, 69, 3350–3361, https://doi.org/https://doi.org/10.1016/j.asr.2022.02.015, 2022.

Rapp, M. and Lübken, F.-J.: Polar mesosphere summer echoes (PMSE): Review of observations and current understanding, Atmospheric Chemistry and Physics, 4, 2601–2633, https://doi.org/10.5194/acp-4-2601-2004, 2004.

Rauf, A., Li, H., Ullah, S., Lin, M., Wang, B., and Wang, M.: Statistical study about the influence of particle precipitation on mesosphere summer echoes in polar latitudes during July 2013, Earth, Planets and Space, 70, https://doi.org/10.1186/s40623-018-0885-6, 2018a.

Rauf, A., Li, H., Ullah, S., Lin, M., Wang, B., and Wang, M.: Investigation of PMSE dependence on high energy particle precipitation during their simultaneous occurrence, Advances in Space Research, 63, https://doi.org/10.1016/j.asr.2018.09.007, 2018b.

Schäfer, B., Baumgarten, G., and Fiedler, J.: Small-scale structures in noctilucent clouds observed by lidar, Journal of Atmospheric and Solar-Terrestrial Physics, 208, 105 384, https://doi.org/https://doi.org/10.1016/j.jastp.2020.105384, 2020.

Shucan, G., Li, H., Xu, T., Zhu, M., Wang, M., Lin, M., Ullah, S., and Rauf, A.: Characteristics of the layered polar mesosphere summer echoes occurrence ratio observed by EISCAT VHF 224 MHz radar, Annales Geophysicae, 37, 417–427, https://doi.org/10.5194/angeo-37-417-2019, 2019.

Singer, W., Hoffmann, P., Grandhi, K. K., Mitchell, N., and Wendt, V.: Atmospheric Coupling by Gravity Waves: Climatology of Gravity Wave Activity, Mesospheric Turbulence and Their Relations to Solar Activity, pp. 409–427, https://doi.org/10.1007/978-94-007-4348-9_22, 2012.

Wilks, D.: Statistical Methods in the Atmospheric Sciences, Academic Press, 100, 50–60, https://doi.org/https://books.google.no/books?id=IJuCVtQ0ySICprintsec=frontcoverhl=frsource=gbs_ge_summary_rcad=0#v=onepageqf=false, 1995.

Zhao, X. R., Sheng, Z., Shi, H. Q., Weng, L. B., and Liao, Q. X.: Long-Term Trends and Solar Responses of the Mesopause Temperatures Observed by SABER During the 2002–2019 Period, Journal of Geophysical Research: Atmospheres, 125, e2020JD032 418, https://doi.org/https://doi.org/10.1029/2020JD032418, e2020JD032418 2020JD032418, 2020.